^{8}B proton halo via reaction and breakup cross section measurements

F. Negoita, C. Borcea, and F. Carstoiu

IAP, P.O. Box MG-6, 76900 Bucharest-Magurele, Romania

M. Lewitowicz, M. G. Saint-Laurent, R. Anne, D. Bazin, J. M. Corre, and P. Roussel-Chomaz

GANIL(IN2P3/CNRS,DSM/CEA) Boîte Postale 5027, 14021 Caen Cedex, France

V. Borrel, D. Guillemaud-Mueller, H. Keller, A. C. Mueller, F. Pougheon, and O. Sorlin

IPN, CNRS-IN2P3, 91406 Orsay Cedex, France

S. Lukyanov, Yu. Penionzhkevich, A. Fomichev, N. Skobelev, and O. Tarasov

FLNR, Joint Institute for Nuclear Research, 141980 Dubna, Moscow Region, Russia

Z. Dlouhy

NPI, 250 68 Rez, Czech Republic

A. Kordyasz

Institute of Experimental Physics, Warsaw University, Hoza 69, 00681 Warsaw, Poland

The reaction cross section for ^{8}B and ^{7}Be and the breakup cross section for ^{8}B on silicon have been measured for incident energies between 10 and 40 MeV/nucleon with a stack of silicon detectors. Secondary ^{8}B and ^{7}Be beams were obtained by use of the LISE spectrometer at GANIL. The stack of silicon detectors had the multiple purpose of slowing down the incident secondary beams, identifying the reaction products, and measuring their energy. The separate contributions of diffraction dissociation and absorption to the breakup have been determined. The parallel momentum distribution of ^{7}Be resulting from the breakup of ^{8}B has also been determined. The data are compared to theoretical calculations. [S0556-2813(96)06009-8]

I. INTRODUCTION

The existence of a proton halo in ^{8}B is a rather controversial question. While the one neutron halo in ^{11}Be and two neutron halo in ^{11}Li are well established by experiment, the evidence for the proton halo is somewhat contradictory. Recent experiments suggest either a large proton halo or a vanishing one.

For example, Minamisono *et al.* [1] found an electric quadrupole moment much larger than the shell model would predict and this was interpreted as a strong evidence in the favor of proton halo. The experimental quadrupole moment could be explained using single particle wave functions (s.p.w.f.) which correspond to a matter density with a radius of 2.7 fm, i.e., much larger than the prediction of any self-consistent calculation. From a measurement of the longitudinal momentum distribution of ^{7}Be after the breakup of ^{8}B (1471 MeV/nucleon) on different targets at GSI, Schwab *et al.* [2] drew conclusions about a large spatial extension of the loosely bound proton in ^{8}B. Indeed, the momentum distribution had a FWHM of 81 MeV/c which implied a radius of 2.78 fm. Similar measurements have been performed quite recently at MSU [3] at lower energies; the widths of the distributions were also small but they show a dependence on the target Z. Recently, Warner *et al.* [4] measured the reaction cross section for ^{8}B + ^{28}Si in the range 30–60 MeV/nucleon, obtaining values around 1.9 b. Again, such large

cross section could be explained by using a density with a radius of 2.7 fm.

These experiments have to be compared with the older result of Tanihata *et al.* [5] who obtained a modest increase of the interaction cross section of ^{8}B as compared with ^{7}Be, the presumable core of ^{8}B. Our previous experiment [6] concerning the quasielastic scattering of ^{7}Be and ^{8}B on a ^{12}C target at 40 MeV/nucleon suggests also that the increase of the optical model reaction cross section is rather consistent with a normal dependence of the interaction radius $R \sim A^{1/3}$. However, the measured angular range for quasielastic scattering was too small to draw definite conclusions about the existence of the proton halo. In particular, as the measured quasielastic cross section does not make a clear separation of the elastic and inelastic components, the deduced reaction cross section is model dependent. Furthermore, the sensitivity of the data with respect to the choice of optical potential has not been studied.

Simultaneously with the quasielastic scattering of ^{8}B and ^{7}Be [6], the excitation function for the breakup reaction ^{8}B + ^{28}Si → ^{7}Be + X was measured. It is believed that such a measurement, due to the very loosely bound nature of the projectile, will provide further information on the proton wave function. The total reaction cross section for ^{8}B + ^{28}Si has also been measured for several energies in the range of 10–40 MeV/nucleon. Complementary measurements of the reaction cross section of ^{7}Be on silicon have been performed in order to have a clear comparison of the

TABLE I. In the second column are given detector thicknesses in μm, the third and fifth columns contain the mean and the variance, in MeV/nucleon, for the distribution of the reaction energies inside the corresponding detector considered as target. σ_R is total reaction cross section on silicon. The one proton breakup cross section of ^{8}B (σ_{bu}) and the separate contributions of diffraction dissociation mechanism (σ_{bu}^{dd}) and absorbtion mechanism (σ_{bu}^a) are given in the last three columns. All the cross sections are in mb.

Det no.	thick.	$E_{\text{reac}}^{7\text{Be}}$	$\sigma_R^{7\text{Be}}$	$E_{\text{reac}}^{8\text{Be}}$	$\sigma_R^{8\text{B}}$	σ_{bu}	σ_{bu}^{dd}	σ_{bu}^a
1	300	38.46 ± 0.56	1491 ± 84	37.96 ± 0.76	1642 ± 75	222 ± 15	112 ± 8	110 ± 9
2	300	36.48 ± 0.58	1476 ± 56	35.23 ± 0.82	1698 ± 70	225 ± 15	130 ± 8	97 ± 8
3	1000	31.80 ± 2.15	1597 ± 56	28.34 ± 3.23	1861 ± 67	244 ± 15	140 ± 8	104 ± 9
4	1000	23.46 ± 2.76	1603 ± 48	15.28 ± 4.88	1940 ± 97			
5	50							
6	50							
7	150							
8	150							
9	300	9.36 ± 1.70	1575 ± 68					
10	300							
11	1000							

core with the presumed halo nucleus. The experimental setup further permitted a determination of the parallel momentum distribution of ^{7}Be resulting from the ^{8}B breakup. All these data taken together impose severe constraints on the theoretical interpretation.

The paper is organized as follows: Section II briefly describes the experimental setup. Section III presents the main features of data reduction: simulations, event identification, cross section and momentum distribution evaluation, together with the results obtained. Section IV is a discussion of the results including a presentation of the main ingredients of the theoretical calculations. The conclusions are summarized in the last section.

II. EXPERIMENTAL SETUP

The general setup and the primary beam characteristics have been described in a previous publication which presented the results on the quasielastic scattering of ^{8}B [6]. Here, only a brief description will be given. A primary beam of ^{13}C (60 MeV/nucleon) with an intensity of 1.4 $e\mu$A delivered by the GANIL cyclotrons impinged on a 2 mm thick ^{9}Be production target. The LISE3 spectrometer was set to select successively ^{8}B and ^{7}Be produced by fragmentation and to form them as secondary beams with an energy of 40 MeV/nucleon. The most important contaminants were ^{7}Be and ^{8}B respectively; they amounted to about 1% of the main beam. All other (lighter) contaminants taken together contributed less than 0.1%. Two parallel plate avalanche counters (PPAC) served to define the ion optics; on them, the beam spot had a diameter of 7 mm. After the second PPAC, a carbon target of 18.5 mg/cm^2 was placed for the quasielastic scattering measurements.

The device that served for measuring the breakup and reaction cross section followed the ideas expounded in [7]. It consisted of a stack of 11 Si detectors which served as target, degrader of beam energy and detecting media for reaction events.

The thicknesses of these detectors are given in Table I. Their frames were 10 mm thick so that the ensemble had a length of about 11 cm. The first detector was x and y posi-

tion sensitive and the second was used for the time of flight (TOF) start signal (the stop signal being provided by the cyclotron radiofrequency) and for triggering the data acquisition. The incident energy of the ^{8}B secondary beam was 320 MeV; after the carbon target the energy was degraded to 314 MeV. At this energy, the corresponding range of ^{8}B in silicon is 2556 μm. Therefore the beam was stopped at the end of the fourth detector (see Table I). This detector is followed by a succession of thin detectors in order to enable the identification of ^{7}Be coming from breakup reactions inside the first four detectors. Because the ^{7}Be produced in breakup has almost the same velocity as ^{8}B but lower charge, it has a longer range in the detector stack than the beam and therefore can be identified in bidimensional plots of energy loss versus residual energy in two successive detectors placed after the fourth one (in which the beam stops).

Extensive simulations have been performed for comparison with, and comprehension of, recorded breakup events. The simulations accounted for the telescope geometry and intrinsic resolution of detectors, energy and angular straggling, energy and angular distribution of the breakup products and different reaction mechanisms. The momentum and position distributions of the incident ^{8}B ions as determined from the experiment were used as initial conditions for the simulated events.

III. DATA REDUCTION

In this section we describe the procedures used to obtain the reaction cross sections, the breakup cross sections and the parallel momentum distributions of ^{7}Be resulting from the one-proton breakup of ^{8}B. The procedures are built as follows: one of the detectors is considered as target and then, the succeeding ones serve to analyze the reaction products thus generated. The cross sections obtained are therefore average values over the range of beam energies inside that detector.

A. Reaction cross sections

The method used for selecting the reaction events is based on the observation that in the detector in which one of the

reactions ^{7}Be+^{28}Si or ^{8}B+^{28}Si took place, the energy deposit is significantly different from that of the beam particles (nonreacted events). Therefore a gate around the typical energy loss of the beam particles in a given detector is sufficient to determine the number of reaction events in that detector and to eliminate them from the flux impinging upon the next one(s).

In the following, the most important factors that can affect the above simple procedure are presented for the ^{8}B beam and for the most affected detector: the first one.

Selections on the position signals have been used to eliminate the eccentric trajectories and consequently, most of the interactions (including diffusion and slowing down) of ^{8}B ions in the materials preceding of the telescope. A gate in TOF corresponding to good ^{8}B values eliminated all the beam contaminants. However, a small number of fragments coming from reactions in the ^{12}C target was still present in telescope. They were identified and eliminated using small area cuts in the bidimensional plots of energy losses in the first two detectors.

The events fulfilling the above conditions are plotted in Fig. 1(a). E_{tot} is the total energy deposit inside the telescope and E_{ini} is the incident energy as deduced from TOF. FD1 is the difference between the recorded energy in the first detector and the calculated energy deposit of a ^{8}B of incident energy E_{ini}. The usefulness of such a representation, as compared with the more common $E1$ vs E_{tot} one, is that it eliminates the incident energy distribution effects. In this figure, the vertical line below the spot of the stopped beam is due to the events channeled in the first detector. The black horizontal strip contains the events passing through the first detector without reacting. The thin lines show the selection criteria for the reaction events in the first detector: $E_{tot}-E_{ini}<-4.7$ MeV and $|$FD1$|>1.5$ MeV.

Of these two conditions, the first one clearly select reactions in the telescope, but may leave outside some of the reactions having a small Q value. The second one is intended to select only the reactions in first detector. The effect of channeling, and to a small extent straggling and intrinsic resolution, may place outside the horizontal band some of the events passing through first detector without reaction, falsely assigning them to the class of reaction events in the first detector. However, these events will react in the next detectors as they fulfill the first condition. Their distribution along the vertical axis is identical to that of nonreacting events ($E_{tot}-E_{ini}>-4.7$ MeV). Based on these arguments, they were subtracted from the number of reactions in the first detector and added to the next ones. Figure 1(b) presents (thick line) the histogram of reaction events in first detector obtained after these corrections.

In order to obtain the reaction cross section from this histogram one has to interpolate over the gate region. The asymmetric, rather peculiar shape of this histogram induced us to make a more detailed analysis. To simplify the interpretation of the histogram in Fig. 1, we eliminated and treated separately an important class of events situated most probably close to the gate: the events corresponding to the ^{8}B$\rightarrow$^{7}Be+p breakup channel, described in next section. The histogram obtained is plotted in the figure as thin line. The shape of this distribution can be readily understood if one takes into account the fact that many reaction events are
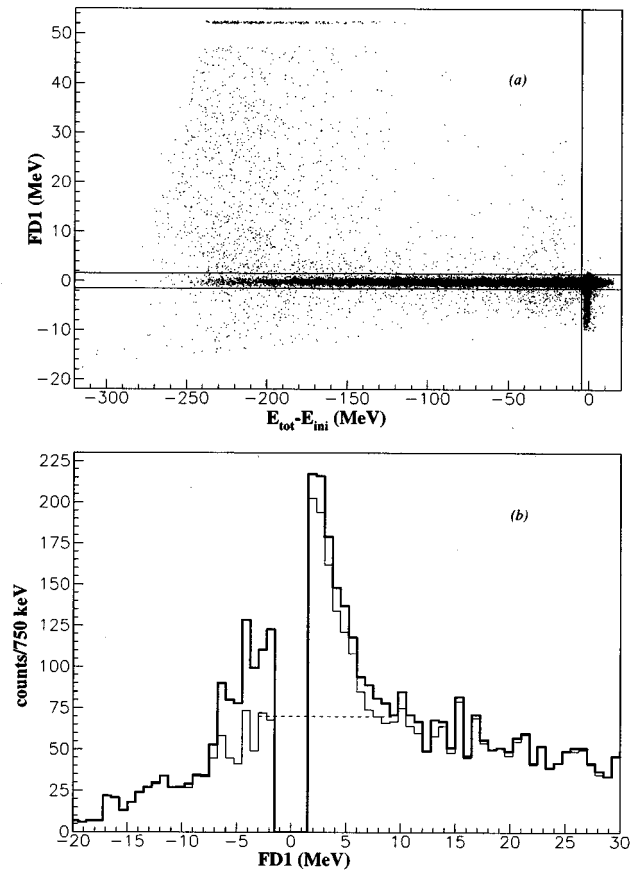

FIG. 1. Experimental spectra used for the determination of the total reaction cross section corresponding to first detector of the telescope (^{8}B beam). E_{tot} is the total energy loss, i.e., the sum of the energy losses in all touched detectors. E_{ini} is the incident energy computed using TOF. FD1=$E1$-$E1^{calc}_{^8B}$ is the difference between the experimental energy loss in first detector ($E1$) and the calculated energy loss ($E1^{calc}_{^8B}$) obtained by forward propagation through the telescope of a ^{8}B of E_{ini} incident energy. (a) Scatter plot of about 5×10^5 incident ^{8}B particles. (b) The histograms of reaction events after channeling correction (thick line) and elimination (thin line) of the events corresponding to the ^{8}B+^{28}Si$\rightarrow$^{7}Be+X breakup channel.

accompanied by light particle emission. Of these particles, some are emitted in the backward direction. If such a particle leaves the reaction detector and penetrates the previous one(s) it will add a supplementary energy to the energy loss of ^{8}B. In Fig. 1, these kind of events occur typically in the interval $0<$ FD1 <7 MeV, producing the observed asymmetry. These events were therefore attributed to other succeeding detectors and the interpolation over the gate was done as shown with the dashed line. Support for this interpretation of the spectrum comes from the fact that the histograms obtained for other detectors, and also for ^{7}Be beam, are very similar. When the backward emitted particle is a proton, it can penetrate more than one detector. Such events were clearly identified and counted as a reaction in the correct detector.

As mentioned above, in the region $E_{tot}-E_{ini}>-4.7$ MeV one can still find reaction events. The events in this region were analyzed in bidimensional plots of energy losses in two

successive detectors. Only a small number of reaction events was found, all of them corresponding to the ^{7}Be$+p$ breakup channel. This analysis, however, cannot be performed for the detector in which the beam stops. Indeed, the reaction products in this case do not have enough energy to pass through the next detector. Therefore, for this detector alone, an extrapolation procedure has been applied.

Thus, the number of the reaction events N_i in the ith detector is determined additively:

$$N_i = N_i^{\text{raw}} + N_i^{\text{chann}} + N_i^{\text{back}} + N_i^{\text{interp}} + N_i^{\text{extrap}} \qquad (1)$$

where the first four terms of the sum stand for raw (uncorrected) reaction number, the corrections due to channeling, backward emitted particles and interpolation inside the gate, respectively. The last one is nonzero, as discussed above, only for the last detector of the beam range.

The resulting reaction cross sections are given in Table I and plotted in Fig. 5: full circles for the ^{8}B beam and open circles for the ^{7}Be beam. Since the uncertainties associated with the last three terms in the above relation do not have a statistical origin, the errors on the number of reactions were computed from

$$\delta N_i = \delta N_i^{\text{raw}} + \delta N_i^{\text{chann}} + \delta N_i^{\text{evap}} + \delta N_i^{\text{interp}} + \delta N_i^{\text{extrap}}.$$

The first two terms were determined from statistical considerations and their contribution to the error represents about 1.5% of the measured cross section, while the total error represents, typically, 5%. The values of the other terms were set according to the limits indicated by different procedures of interpolation and extrapolation.

One notes that the inelastic channel and the neutron emission channels do not lead to a sensitive change in energy loss in the reaction detector and therefore are beyond the sensitivity of the present method. However, the cross section for neutron emission channels alone (without other charged particles or fragments) is almost negligible at the involved energies and the estimated inelastic cross section (as in Ref. [6]) is only 20 mb.

B. Proton breakup cross sections

In this section, a breakup event is defined as one in which an incident ^{8}B ion propagates through the telescope up to a given depth, after which it turns into a ^{7}Be ion that will continue propagating up to the end of its range. However, in order to identify the ^{7}Be, it must penetrate through at least two detectors before reaching the end of its range. Only in this case can it be identified in the $(\Delta E, E_{\text{res}})$ plot built for the last two detectors before it stopped. Therefore many breakup events occurring in the fourth detector were not identified and the breakup cross section was determined only for the first three detectors.

About a quarter of the total number of the selected breakup events are plotted in Fig. 2(a). The vertical axis has the same meaning as in the plots used for total reaction cross section. The ^{8}B particles passing through the first detector without reaction are located on the horizontal strip around FD1=0 MeV. The horizontal axis (see caption) gives the deviation of the measured sum of energy losses in the second and third detectors from the expected energy loss of a ^{7}Be
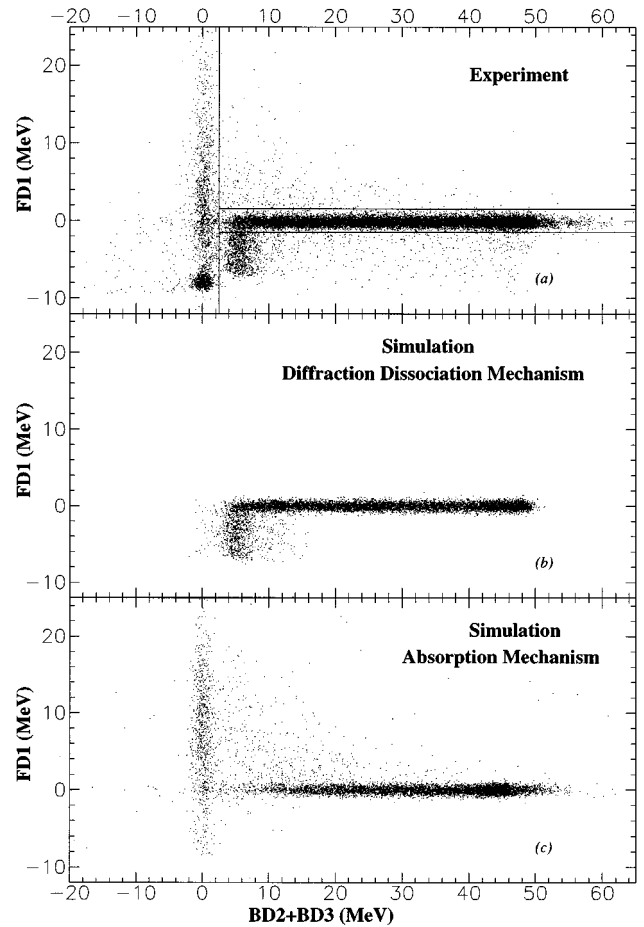

FIG. 2. Experimental (a) and simulated (b),(c) diagrams used for breakup cross section evaluation. BD2$=E2-E2_{^7\text{Be}}^{\text{calc}}$ is difference between the experimental energy loss in the first detector ($E2$) and the calculated energy loss ($E2_{^7\text{Be}}^{\text{calc}}$) obtained by backward propagation through the telescope of a ^{7}Be from the last touched detector (and its energy signal) till the first one. (a) Scatter plot of about 2×10^5 events identified as ^{7}Be in last two detectors of the trajectory. (b) Simulated events corresponding to diffraction dissociation breakup mechanism. (c) Simulated events corresponding to absorption breakup mechanism.

coming from a reaction in the first detector. A negative deviation occurs when a ^{7}Be fragment is channeled and a positive deviation when a ^{7}Be is accompanied by another reaction product. The other events lie on the vertical strip (at the left of the vertical line) whose width is determined only by the straggling and the intrinsic resolution of second and third detectors.

The spot in the left-bottom corner of the figure represents the ^{7}Be produced in breakup reactions in front of the telescope. Their number is large because, from the selections mentioned in the beginning of the Sec. III A, we kept only the TOF gate in the selection criteria. But they are well separated from the breakup events inside the telescope and are even better separated in a slightly changed representation in which the FD1 axis is replaced by BD1.

Figure 2(b) presents some simulations done assuming that the two breakup fragments, ^{7}Be and the proton, were for-

wardly emitted with a certain velocity distribution in the center of mass of ^{8}B. Consequently, the energy loss in the detector in which the reaction took place decreased compared to a noninteracting ^{8}B, and the proton energy loss has then been added to the energy loss of ^{7}Be in next detectors. We associate these events to the *diffraction dissociation* breakup mechanism. The experimental events situated at the left of the vertical line [Fig. 2(a)] have, however, a different behavior: a large excess in their energy loss is recorded and the ^{7}Be fragment propagates alone in next detectors. These events correspond to the *absorption* breakup mechanism in which the valence proton of ^{8}B suffers a strong interaction with the target while the ^{7}Be core continues to move along the telescope.

In order to simulate also the breakup events corresponding to the absorption mechanism, we supposed that the interaction between the proton and the target nucleus is a fusion-evaporation reaction. Therefore an evaporation code has been included. The excitation energy of the ^{29}P compound nucleus has been calculated from momentum and energy conservation. Its spin was set to different values, in an attempt to reproduce the distribution of energy losses in the reaction detector and the number of events in which the evaporated particles pass from one detector to the other. The result of such a simulation is plotted in Fig. 2(c). One may observe that the sum of the two simulations (i.e., absorption plus diffraction dissociation breakup mechanisms), presented in Figs. 2(b) and 2(c), qualitatively reproduce the experimental distribution in Fig. 2(a). However, the energy excess found in these simulations was smaller than the observed experimental one and the number of evaporated particles as given by the simulations was larger than the real one. This suggests that other mechanisms are also important in the proton target interaction.

The total breakup cross sections and the cross sections corresponding to the two breakup components were obtained after the evaluation of the correction terms contained in the expression (1). The results are given in Table I and are plotted in Fig. 6. The contribution of statistics to the error bars is even smaller than in the case of total reaction cross section.

A special simulation was done in order to evaluate the number of ^{7}Be which may have escaped from the telescope. The Coulomb deviation was determined for a distribution of the impact parameters leading to breakup obtained from a theoretical calculation (see below). A Lorentzian distribution with $\Gamma = 93$ MeV/c has been considered for the momentum of ^{7}Be resulting from breakup (see Sec. III D). The incident energy and momentum distribution of ^{8}B were those from the experiment. The resulting number of escapes was less than 0.7% of the total number of generated events and therefore this correction is considered as a negligible one.

C. Other breakup channels

The telescope used in the present experiment has not been designed to stop lower Z products ($Z=2,3$). However, using the second detector as target and the two following ones as transmission detectors, Li and He ions can be identified by their characteristic energy losses in these two detectors. The accompanying protons that lose little amounts of energy do not alter this transmission identification pattern. Therefore,

the cross sections for the following breakup channels could be determined: ^{7}Be$\rightarrow$^{3}He+^{4}He: 242 mb, ^{7}Be$\rightarrow$^{6}Li+p: 168 mb, ^{8}B$\rightarrow$^{3}He+^{4}He+p: 178 mb and ^{8}B$\rightarrow$^{6}Li+p+p: 154 mb.

The values obtained are rather lower limits because the situations in which the He or Li ion was accompanied by a heavy target fragment, lead to an extra energy deposit in detectors 3 and/or 4, thus excluding them from the transmission patterns.

The large cross sections for the He breakup channels seems to add support for the supposed cluster structure of ^{7}Be [8]. However, the striking feature of these results is the important decrease of the cross section for the He breakup channel when passing from ^{7}Be to ^{8}B. This fact indicates a different behavior of the ^{7}Be when it is considered as the core of ^{8}B.

D. Momentum distributions

The momentum distribution of the ^{7}Be fragments has been determined for the first detector taken as target, i.e., for a mean incident ^{8}B energy of 38 MeV/nucleon. For the events selected in the first detector as absorption breakup (according to the description in Sec. III B), the distribution of the sum of energies left in all subsequent detectors was made; it is shown (full squares) in Fig. 3.

In the laboratory system the momentum and the energy of ^{7}Be can be written

$$\vec{p}_7^{\,\text{lab}} = \vec{p}_0 + \vec{p}, \quad E_7^{\text{lab}} = \frac{1}{2m_7}(\vec{p}_0^{\,2} + 2\vec{p}_0\vec{p} + \vec{p}^{\,2}),$$

where $\vec{p}$ is the ^{7}Be momentum in the center of mass of ^{8}B and $\vec{p}_0$ corresponds to the c.m. velocity: $\vec{p}_0 = m_7/m_8 \vec{p}_8^{\,\text{lab}}$.

At a fixed reaction energy, the variance of the energy distribution of the ^{7}Be fragments, irrespective of the momentum distribution is given by

$$\sigma_{E_7^{\text{lab}}}^2 = \left(\frac{1}{2m_7}\right)^2 [4p_0^2 \sigma_{p_z}^2 + \sigma_{p^2}^2 + 4p_0(\overline{p_z p^2} - \overline{p_z}\,\overline{p^2})],$$

in which the z direction is taken along $\vec{p}_0$. The last term vanishes for isotropical distributions; the second term is very small compared to the first one since p_0 is about 1800 MeV/c for the reactions in first detector. Therefore, the width of the measured energy distribution is sensitive only to the parallel momentum distribution of ^{7}Be in the center of mass of ^{8}B.

To reproduce the experimental pattern in Fig. 3, events were simulated (as described previously) using tridimensional momentum distributions ($\vec{p}$) of both Gaussian and Lorentzian forms. A χ^2 test is defined as the sum of squares of differences between the bin content of experimental and simulated histograms. The best fit is obtained for a Lorentzian distribution with $\Gamma = 93 \pm 7$ MeV/c and the corresponding histogram is given by the thick line in Fig. 3. The thin line histogram in Fig. 3 is the result of a simulation where Γ is set to zero and shows the contribution of the incident energy distribution, the intrinsic resolution as well as that of straggling and of the wide range of reaction energies to the total distribution. The above result is consistent with that of Schwab *et al.* [2], obtained at a much higher incident energy.
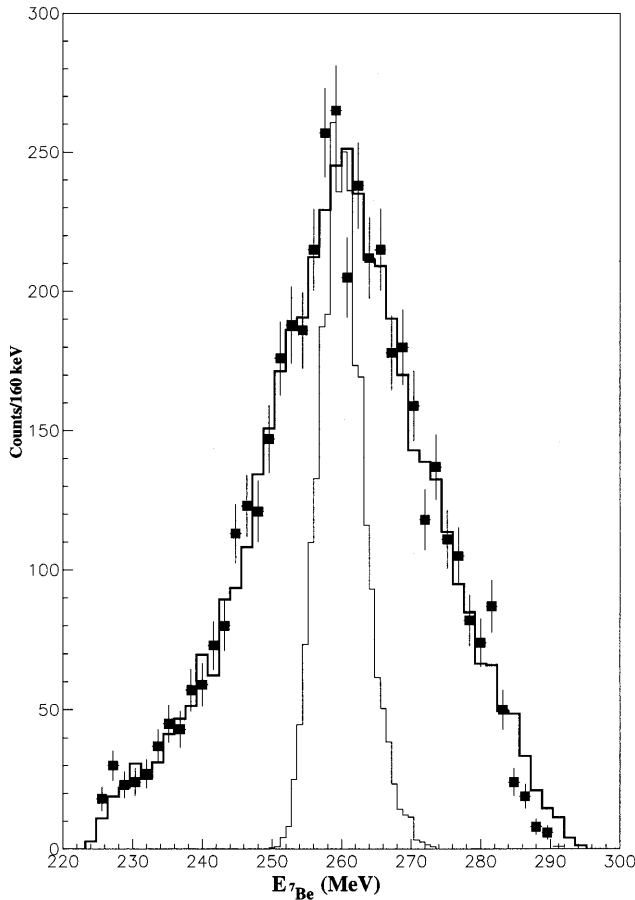
FIG. 3. The points represent the experimental distribution of the energy of the ^{7}Be breakup fragment at the exit from the reaction detector (the sum of energy losses in next detectors). The histograms represent the same distribution for simulations using a Lorentzian distribution of the ^{7}Be momentum in the c.m. of ^{8}B with $\Gamma = 93$ MeV/c (thick line) and $\Gamma = 0$ MeV/c (thin line).

This determination refers to the absorption breakup mechanism. To apply the procedure to the diffraction dissociation component is hazardous because the energy added by the accompanying proton may alter the results. However, a close examination showed that the stopping length distributions of ^{7}Be coming from the two mechanism are almost identical. These distributions are not affected by the accompanying proton, but are enlarged by straggling. The straggling contribution can be evaluated from that of the incident ^{7}Be beam, and is much smaller that the contribution of the parallel momentum distribution. The resemblance of the two stopping length distributions is therefore a strong argument for the identity of the momentum distributions of the two mechanisms.

IV. DISCUSSION

Perhaps the most striking features of the present experimental data are the following: large reaction cross sections for ^{8}B and ^{7}Be, as expected for loosely bound nuclei; almost equal contributions to the one proton breakup cross section of ^{8}B coming from diffraction dissociation and from absorption; the one proton breakup cross section for ^{8}B equals, to a

good approximation, the difference between the reaction cross sections of ^{8}B and that of ^{7}Be:

$$\sigma_{-p} = \sigma_R(^8\text{B}) - \sigma_R(^7\text{Be}), \tag{2}$$

i.e., the ^{8}B nucleus has the same separability property observed for typical halo nuclei like ^{11}Li and ^{11}Be.

This property imposes severe constraints on the theoretical models used to explain the data. Qualitatively, the last feature in the above list can be understood using simple geometrical arguments. The impact parameter introduced by the relation:

$$\sigma_R = \pi b_c^2 \tag{3}$$

defines an interaction region, inside of which nearly all collisions will lead to reaction events. Due to the very small one proton separation energy, only the outermost impact parameters in the interaction region will lead to the proton breakup, while for smaller impact parameters, and implicitly for more violent collisions, other channels will dominate the reaction cross section. Therefore, the proton breakup cross section is essentially determined by impact parameters in a thin layer Δb centered around the critical value b_c and

$$\sigma_{-p} = 2\pi\left(b_c - \frac{\Delta b}{2}\right)\Delta b \tag{4}$$

which has the same meaning as Eq. (2). Using Eqs. (3) and (4) and our reaction and breakup cross sections at 35 MeV/nucleon one obtains $b_c = 7.50 \pm 0.14$ fm and $\Delta b = 0.51 \pm 0.07$ fm. For comparison, we have extracted from the data of Fukuda *et al.* [9] for ^{11}Be + ^{27}Al (33 MeV/nucleon) the following values: $b_c = 8.50 \pm 0.09$ fm and $\Delta b = 1.32 \pm 0.66$ fm. The large difference in Δb shows clearly that the proton breakup cross section for ^{8}B is dominated by contributions coming from a small range of impact parameters and that the valence proton wave function (w.f.) has a smaller spatial extension as compared to, e.g., the ^{11}Be case.

In the following we describe briefly the procedure to obtain the w.f. and densities for ^{7}Be, ^{8}B, and ^{28}Si, which are necessary in order to interpret the experimental data.

A. Model wave functions

The target (^{28}Si) and the core (^{7}Be) densities were obtained in a standard spherical Hartree-Fock (HF) calculation using the Skyrme II parametrization of the effective interaction. For ^{7}Be the calculation was constrained to reproduce the experimental binding energy by a renormalization procedure of the effective interaction.

For ^{8}B, calculations with microscopic cluster models [10,11] suggest that the ^{7}Be + p configuration has a large overlap with the total w.f. of the ^{8}B and the tail of the proton density is dominated by the slow decrease of the ^{7}Be + p relative w.f. Though this large overlap may be taken as an argument for a mean field calculation (e.g., HF with Skyrme type effective interaction) the total binding energies thus obtained disagree by 1 to 5 MeV with respect to the experiment. Therefore such models cannot be used without a con-

TABLE II. Values of proton, neutron, and matter radii (r_p, r_n, r_m) and proton skin $(r_p - r_n)$ in fm.

Nucleus	r_p	r_n	r_m	$r_p - r_n$	Model
⁷Be	2.369	2.155	2.280	0.214	HF SkII
⁸B	2.754	2.267	2.582	0.487	HF SkII+SM
	2.759	2.155	2.549	0.604	HF SkII mean field+
					$\epsilon_{1p_{3/2}} = -0.137$ MeV
	2.790	2.247	2.600	0.543	WS, $\beta = 0.6$
	2.74	2.25	2.57	0.49	RGM [10]
	2.88	2.47	2.73	0.41	GCM [11]
²⁸Si	3.061	3.025	3.043		HF SkII

straint on the binding energy. Also, configuration mixing plays an important role. In order to fulfill these requirements for ⁸B, a self-consistent calculation of single particle wave functions has been performed using shell model (SM) occupation probabilities and a constraint on the total binding energy. This procedure is essentially the method (ii) described by Hoshino, Sagawa, and Arima in their Appendix A1 [12]. The SM occupation probabilities were obtained as described previously [6] and the HFSK II w.f. were used to construct the one body densities in the configuration space.

In order to get more flexibility for the valence proton w.f., we have used the well depth (or Sturm-Liouville) method that successfully explains the reaction cross section of the halo nuclei [13]. As a reference potential we have taken the HF SkII mean field potential (including the Coulomb barrier) and the proton valence binding energy fixed at $\epsilon_{1p_{3/2}} = -0.137$ MeV. Then, the total ⁸B density was obtained by adding the valence density

$$\rho_{\text{val}}(r) = \frac{1}{4\pi} \psi_{1p_{3/2}}^2(r)$$

to the density of the core. It should be noted that the angular part is dropped since, as shown in Ref. [14], the reaction and breakup cross sections depend weakly on the angular part of the valence density. Table II presents the radii obtained from the densities described above.

The large experimental value of the ⁸B quadrupole moment [1] suggests that the deformation may be rather important. Therefore, an adequate calculation has been performed as described in [15], assuming axial symmetry and a single particle Hamiltonian with Woods-Saxon form factors. In order to obtain a r.m.s. radius comparable to the preceding calculations a deformation $\beta = 0.6$ had to be chosen. The results are displayed in Table II and Fig. 4. The r.m.s. radii are similar with the results of microscopic RGM [10] and GCM [11] calculations. To a good approximation, the well depth method reproduces the RGM results. However, the pattern of this density in the asymptotic region differs substantially from that produced by the large deformation.

For further analysis, at this point it is useful to define the decay length (α) of the wave function in the asymptotic region by the use of a simple Yukawa form factor:

$$\psi = \frac{1}{\sqrt{2\pi\alpha}} \frac{e^{-r/\alpha}}{r}, \quad \alpha = \sqrt{\frac{\hbar^2}{2\mu S_{\text{eff}}}}. \quad (5)$$
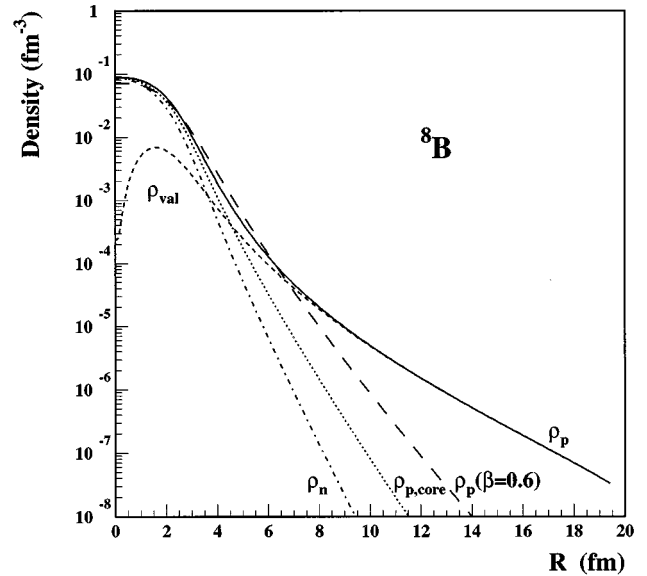

FIG. 4. Radial dependence of the ⁸B one body densities. The valence density (short-dashed) is obtained with the well depth method using the HF SkII mean field (including the Coulomb term) as a reference potential and $\epsilon_{1p_{3/2}} = -0.137$ MeV. The core neutron (dash-dotted) and proton (dotted) densities are obtained with HF SkII and a constraint on the total binding energy. The total proton density is obtained from core and valence components. The deformed WS ($\beta = 0.6$) proton density is also shown (long dashed).

We have obtained the following values: $\alpha = 3.97$ fm for the HF density and $\alpha = 1.986$ fm for the deformed density. We shall see below that the experimental data clearly distinguish between the two densities, favoring the HF one.

B. Reaction and breakup cross section

The measurement of the reaction and breakup cross sections provide useful information about the size of unstable nuclei. Especially the breakup cross section should be in principle sensitive to the asymptotic behavior of the wave function for nuclei with small nucleon separation energy. The geometrical character of the cross section is revealed by the impact parameter representation of the scattering amplitude:

$$\sigma_R = \int d\vec{b} [1 - \exp(-2 \operatorname{Im}\chi(b))]. \quad (6)$$

At intermediate and high energies, the phase shift function $\chi(b)$ can be calculated in the Glauber model [16]. At low energies, medium effects become important and we have to deal with effective forces. In principle, coupling to the excited states should be also included. The problem of extending the Glauber calculations at low energies has been considered in a number of papers [17–19]. It was shown that the eikonal approximation can still be used, provided proper corrections are applied. More specifically, for the total and reaction cross section it was demonstrated [19] that the eikonal expansion that includes corrections up to the second order converges rapidly toward the full quantum mechanical result.

As in a previous paper [6] we suppose that, in the eikonal approximation, the phase shift function (eikonal phase) can be generated by an optical potential

$$\chi(b) = \sum_{\alpha\beta} \chi_{\alpha\beta}(b), \quad \alpha,\beta = \text{proton, neutron,}$$

$$\chi_{\alpha\beta}(b) = \frac{i}{2}\sigma_{\alpha\beta}\int d\vec{b}_1\, d\vec{b}_2\, \rho_{1\alpha}(b_1)\rho_{2\beta}(b_2)f(\vec{b}_1 + \vec{b} - \vec{b}_2),$$
(7)

where $\rho_{i\alpha(\beta)}$ are the profile density functions and the free nucleon-nucleon interaction cross section $\sigma_{\alpha\beta}$ are used at an appropriate energy. The smearing function f accounts for finite range (f.r.) and medium effects which are the most important corrections at low energies. According to [13] this function is taken in a gaussian form with a range $b_0 = 1$ fm. The zero range (z.r.) approximation, widely used at high energies, is obtained in the limit $b_0 \rightarrow 0$. We neglect for the moment the refractive effects arising from the real part of the optical potential, therefore the eikonal phases are purely imaginary.

To describe the one proton breakup process we follow the prescription of Bertsch *et al.* [20]. The projectile one body density is decomposed into the core and valence components, and the eikonal phases are calculated using appropriate kinematics. Since all excited states of ^{8}B are particle unstable, we assume that any excitation of the valence nucleon will contribute to the breakup channel. In this approximation, the breakup is considered as a direct process and multistep effects such as resonant breakup are ignored.

With the above approximations, the one nucleon breakup probability is written as

$$P_{-p}(b) = [1 - \exp(-2\,\text{Im}\chi_{\text{val}}(b))]\exp(-2\,\text{Im}\chi_{\text{core}}(b)),$$
(8)

the first factor representing the probability for excitation of the valence nucleon to a continuum state, and the second one is nothing but the survival probability of the core after the interaction with the target. This last term must be present, since in an inclusive experiment the core is detected in a particle stable state. The total cross section is obtained by integrating over the impact parameter.

A significant improvement in the agreement with the data can be obtained by refining the above calculations, such as to take into account the refractive and the density dependence effects. This can be achieved by performing a full quantum optical model calculation for the cross section. The optical potentials were generated using the complex density and energy dependent effective interaction of Jeukenne, Lejeune, and Mahaux (JLM) [21]. The double folding form factors were renormalized by a unique couple of multiplicative constants $N_V = 0.65$ and $N_W = 0.80$ obtained by fitting elastic scattering data ^{6}Li$+^{28}$Si in the range $15-53$ MeV/nucleon [22].

Our data provided unique information about the diffraction dissociation and absorption contributions to the total breakup cross section. The optical model does not allow an easy evaluation of these components. Therefore, the extended Serber model as formulated in [23] has been used. Originally, the model was designed to describe the one neu-

tron removal cross section for the halo nucleus ^{11}Be. The model uses only the asymptotic part of the intruder state $s_{1/2}$ taken in Yukawa form (5). For the ^{8}B case, the model can be naturally extended by allowing the effective separation energy to include Coulomb and centrifugal effects:

$$S_{\text{eff}} = \epsilon_{p_{3/2}} + B_c + B_l,$$

where B_c and B_l are the Coulomb and centrifugal energies at the top of s-wave mean field potential. This is consistent with the result of Lassaut and Lombard [24] obtained in the inverse scattering theory.

C. Comparison with experimental data

The experimental data and theoretical calculations are displayed in Figs. 5 and 6. It is to be noted that, for a given target density, the ^{7}Be reaction cross section depends essentially only on the core density, while the ^{8}B reaction and one proton breakup cross sections involve also the valence density. Furthermore, the diffraction dissociation and absorption components of the breakup cross section are very sensitive to the asymptotic behavior of the valence wave function. Therefore, only a consistent description of all data allows the extraction of a meaningful information about the size of the ^{8}B nucleus.

As can be seen in the figures, the optical model calculation accounts very well for both the magnitude and the energy dependence of the cross sections. In the Glauber model, the cross sections are scaled by the r.m.s. radius of the eikonal phase and this explains the large difference between the f.r. and the z.r. calculation. Therefore, the z.r. approximation should be used with caution in the low energy region, when size information is to be inferred from the reaction cross section alone. At high energies, the cross section is dominated by NN collisions and medium and finite size effects are less important.

The extended Serber model accounts well for the magnitude of the breakup cross section, while the energy dependence is slightly underestimated. In this model the energy dependence comes from the diffraction dissociation component alone. Although we have not enough evidence, the data seem to suggest a slight decrease with energy of the absorption breakup cross section. However, more experimental information is needed to clarify this point.

We have used the above models to determine the sensitivity of the cross section to the size parameters. A series of valence densities were generated with the well depth method by fixing the single particle energy in the range from -5 to 0 MeV. Then the total breakup cross section was calculated as above, using JLM and Glauber zero range formula. The patterns thus obtained are presented in Fig. 7. In the region of interest, a weak model dependence of the cross section is found. This allows us to extract an r.m.s. radius for the valence density of 3.97 ± 0.12 fm as determined by one standard deviation in the experimental data. Combining this value with the core radii from Table I, we obtain $r_p = 2.76 \pm 0.08$ fm and $r_m = 2.55 \pm 0.08$ fm.

A similar analysis was performed within the Serber model using the decay length α (or, equivalently, the effective separation energy S_{eff}) as a control parameter. The χ^2 test based
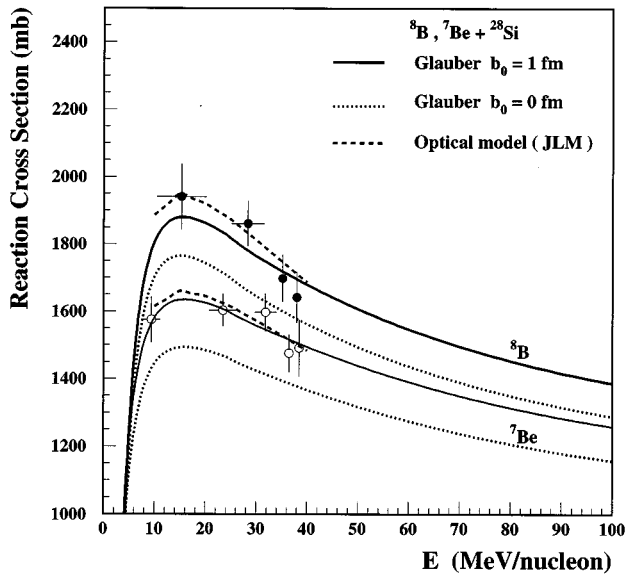
FIG. 5. The energy dependence of experimental reaction cross section of ^{7}Be and ^{8}B$+^{28}$Si are compared with zero range (dotted line) and finite range (continuous line) Glauber model and with JLM optical model (dashed line). All calculations are done using the proton valence and the core densities shown in Fig. 4.
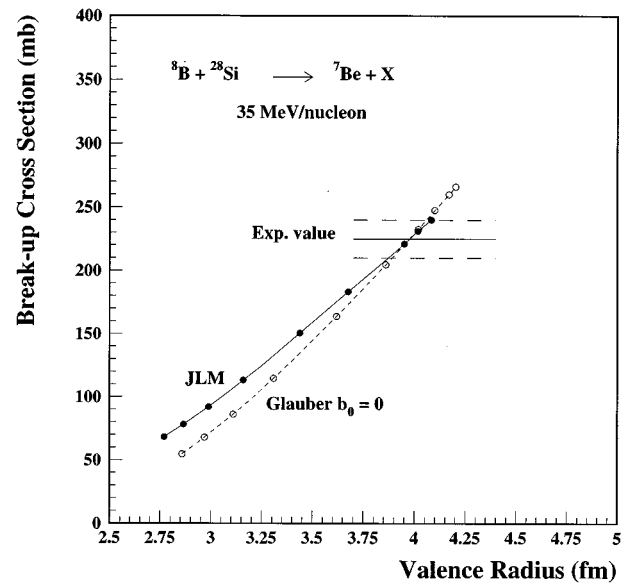

FIG. 7. The total breakup cross section as a function of the proton valence r.m.s. density radius. The lines joining the points are obtained using $\epsilon_{1p_{3/2}}$ from -5 to 0 MeV in the well depth method. The JLM optical model (full circles) and the Glauber model (open circles) are used for cross sections.

on all breakup data (the insert in Fig. 8) shows a high selectivity on the control parameter and provides the following values: $\alpha=4.13\pm0.15$ fm and $S_{eff}=1.38\pm0.1$ MeV. These results are in excellent agreement with the HF w.f. and clearly invalidate the asymptotic pattern of a deformed density. The Lorentzian momentum distribution derived from the Yukawa w.f. (5) with the above decay length has then a width $\Gamma=95$ MeV/c, close to the experimentally measured value.

In Figs. 9 and 10 the experimental data of Refs. [2,4,5] have been summarized and compared with a Glauber model calculation. The z.r. approximation accounts well for both reaction and breakup cross sections measured by Schwab *et al.* at 1.4 GeV/nucleon, but slightly overestimates (by 7%) the data at 0.8 GeV/nucleon of Tanihata *et al.* [5]. We have also recalculated the elastic scattering of ^{7}Be, ^{8}B $+$ ^{12}C at 40 MeV/nucleon using the present w.f. The

FIG. 6. The experimental total breakup cross sections (full circles) and the diffraction (triangles) and absorption (open circles) components are compared with Glauber, Serber, and JLM optical model.
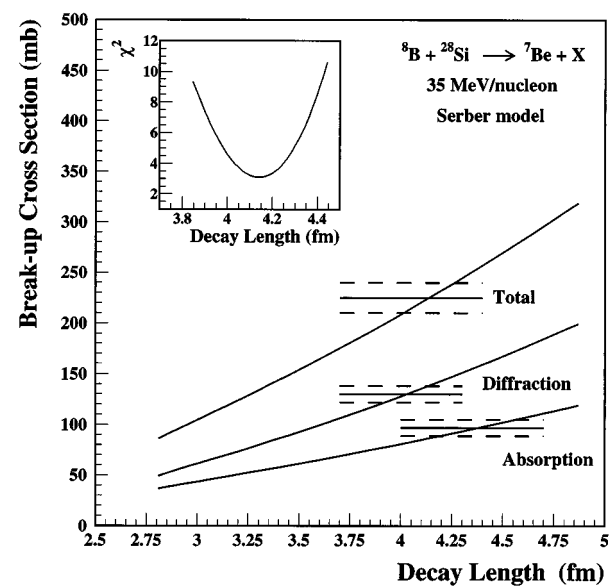

FIG. 8. The total breakup cross section, and the diffraction and absorption components as a function of the decay length of the proton valence w.f. (obtained as for Fig. 4). The insert shows the sensitivity of the χ^2 upon the control parameter.
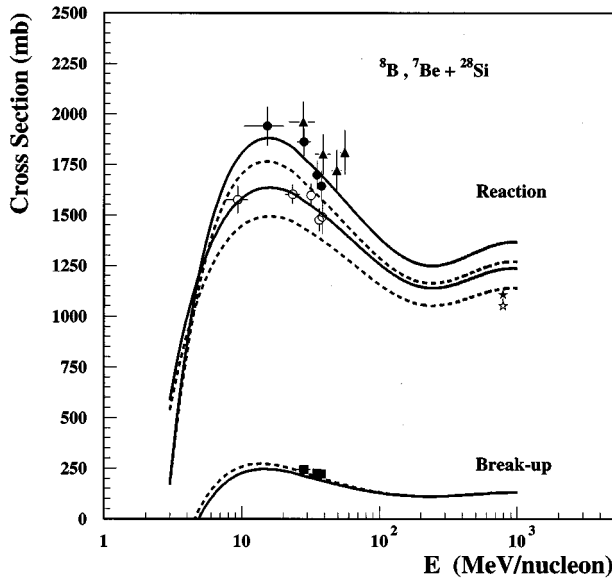
FIG. 9. Summary of the existing reaction and breakup cross sections on a ^{28}Si target. Data of Warner *et al.* [4] are shown by triangles. The interaction cross sections of Tanihata *et al.* [5] on an Al target are shown by stars. Data are compared with a finite range (full line) and zero range (dotted line) Glauber model calculation.

results displayed in Fig. 11 show little difference with respect to the previous calculation, confirming the relative insensitivity of the elastic scattering data to the choice of the w.f.

The width of the longitudinal momentum distribution obtained from the Fourier transform of the proton valence w.f. is about 150 MeV/c, i.e., much larger than the experimental
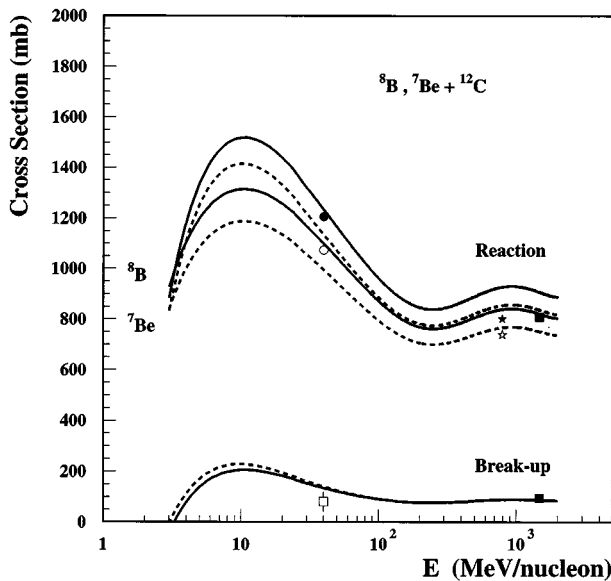

FIG. 10. The same as in Fig. 9 for ^{12}C target. Data of Schwab *et al.* [2] (full squares), Pecina *et al.* [6] (open square), and of Tanihata *et al.* [5] (stars) are compared with Glauber model. The results of a JLM optical model calculation (circles) at 40 MeV/nucleon are also shown (see also Fig. 11).
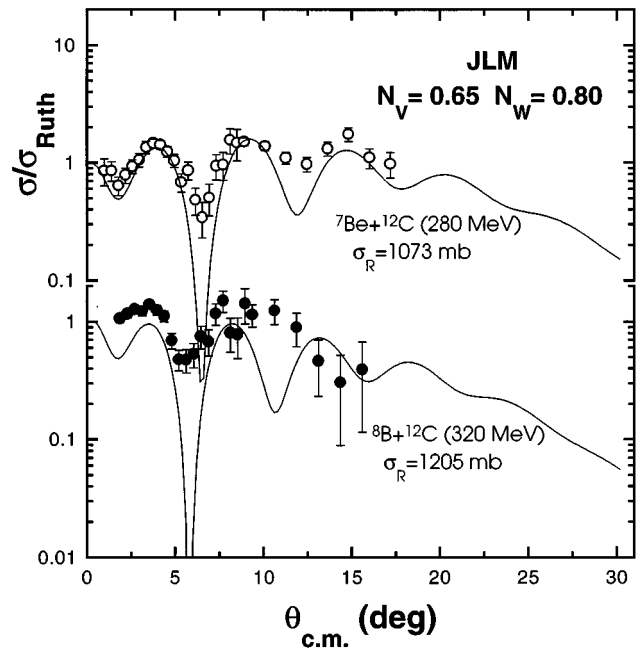

FIG. 11. The quasielastic scattering data of Pecina *et al.* [6] are compared with a JLM optical model calculation.

data: 93 MeV/c. In our experiment, the longitudinal momentum distribution has been determined by measuring the ^{7}Be momentum after the breakup. ^{7}Be is itself a rather loosely bound nucleus and one expects that the measured distribution scans mostly the surface region as suggested by the models of Friedman [25], Hüfner and Nemes [26], and Hussein and McVoy [27]. The separability property, Eq. (2), well verified by the data, indicates that essentially impact parameters around 7.5 fm contribute to the breakup. However, the relationship between the impact parameter and the cutoff radius is not straightforward. A cutoff radius $r_{cut}=5$ fm leads to an excellent agreement with the measured width of the momentum distribution. The physical meaning of the cutoff procedure resides in the relative independence of the cross sections on the r_{cut}: for $r_{cut}=5$ fm the breakup cross section diminishes by 25%, the reaction cross section by only 3% while the norm of the valence proton density drops by 82%. This clearly shows that only the tail of the valence w.f. is important for the breakup process and that 5 fm is a reasonable value for r_{cut}.

D. Astrophysical aspects

The structure of ^{8}B is very important in connection with the astrophysical problem of solar neutrinos. The good agreement with the experimental data of the present optical model calculations give us confidence in the obtained w.f. Recently, Brown, Csótó, and Sherr [28], deduced a theoretical relation between the absolute normalization of the proton valence density (i.e., the density value at $r=10$ fm) and the astrophysical S_{17} factor for the ^{7}Be(p,γ) reaction:

$$S_{17}(20 \text{ keV})=2.99\times10^6\rho(10 \text{ fm})S,$$

where S is the spectroscopic factor. Using our value $\rho(r=10 \text{ fm})=5\times10^{-6} \text{ fm}^{-3}$ and the spectroscopic factor

calculated by Brown *et al.* [28] one obtains $S_{17}=17.2$ eV b. This is identical with the recent value obtained by Barker in an *R*-matrix approach [29].

V. CONCLUSIONS

Knowledge about ^{8}B nucleus is valuable both for astrophysical reasons and for clarifying the question of the existence of proton halo. An efficient experimental setup permitted us to obtain simultaneously a large amount of information: reaction and breakup cross sections at several energies and longitudinal momentum distributions. In addition, the diffraction dissociation and absorption components of the breakup cross section have been determined. All these data impose severe constraints on theoretical models and only a consistent description of the whole body of data allows the extraction of a meaningful information on the size parameters of the ^{8}B nucleus. The ensemble of data can be well reproduced by using w.f. obtained from a H.F. calculation, which was in turn constrained to reproduce the experimental binding energy and shell model occupation probabilities. The less conventional well depth method proved to be useful in clarifying the role of Coulomb and centrifugal potentials for the asymptotic behavior and for the confinement of the proton valence w.f. inside the barrier. This leads to the formation of a weakly developed proton halo ("pigmy halo") or equivalently to a substantial proton skin. A large deformation could also play a key role in understanding the structure of ^{8}B. However, a crude estimation of this effect based on a rather uncertain Woods Saxon deformed potential leads to a proton valence w.f. which decreases too steeply in the asymptotic region and does not fit well the present experimental data. The astrophysical factor S_{17} amounts to 17.2 eV b and thus is consistent with other theoretical estimates, but is lower by 20% than the weighted average of previous experimental data [30].

Though a by-product of the present measurements, the important variation in the relative weight of the breakup channels with ^{3}He/^{4}He production when passing from ^{7}Be to ^{8}B deserves further study.

ACKNOWLEDGMENTS

[1] T. Minamisono *et al.*, Phys. Rev. Lett. **69**, 2058 (1992).

[2] W. Schwab *et al.*, Z. Phys. A **350**, 283 (1995).

[3] J. Kelley, Ph.D. thesis, Michigan State University, 1995; (private communication).

[4] R. E. Warner *et al.*, Phys. Rev. C **52**, R1166 (1995).

[5] I. Tanihata, H. Hamagaki, O. Hashimoto, Y. Shida, N. Yoshikawa, K. Sugimoto, O. Yamakawa, T. Kobayashi, and N. Takahashi, Phys. Rev. Lett. **55**, 2676 (1985); I. Tanihata, T. Kobayashi, O. Yamakawa, S. Shimoura, K. Ekuni, K. Sugimoto, N. Takahashi, T. Shimoda, and H. Sato, Phys. Lett. B **206**, 592 (1988); M. M. Obuti, T. Kpobayashi, D. Hirata, Y. Ogawa, A. Ozawa, K. Sugimoto, I. Tanihata, D. Olson, W. Christie, and H. Wieman, Report No. RIKEN-AF-NP-227 (1996).

[6] I. Pecina *et al.*, Phys. Rev. C **52**, 191 (1995).

[7] J. M. Corre *et al.*, Nucl. Instrum. Methods A **359**, 511 (1995).

[8] Y. Kanada-En'yo, H. Horiuchi, and A. Ono, Phys. Rev. C **52**, 628 (1995).

[9] M. Fukuda *et al.*, Phys. Lett. B **268**, 339 (1991).

[10] A. Csótó, Phys. Lett. B **315**, 24 (1993).

[11] D. Baye, P. Descouvremont, and N. K. Timofeyuk, Nucl. Phys. **A577**, 624 (1994).

[12] T. Hoshino, H. Sagawa, and A. Arima, Nucl. Phys. **A596**, 271 (1990).

[13] G. F. Bertsch, B. A. Brown, and H. Sagawa, Phys. Rev. C **39**, 1154 (1989); B. A. Brown, E. K. Warburton, and B. H. Wildenthal, in *Proceedings of the Workshop on Nuclear Structure of Light Nuclei far from Stability. Experiment and Theory*, Obernai, 1989, edited by G. Klotz (Kuster, Strasbourg, 1991).

[14] B. V. Carlson, Phys. Rev. C **51**, 252 (1995).

[15] S. Cwiok, J. Dudek, W. Nazarewicz, J. Skalski, and T. Werner, Comput. Phys. Commun. **46**, 379 (1987).

[16] R. J. Glauber, *Lectures in Theoretical Physics*, edited by W. E. Brittin (Interscience, N.Y., 1959), Vol. I.

[17] S. M. Lenzi, A. Vitturi, and F. Zardi, Z. Phys. A **352**, 303 (1995).

[18] G. Fäldt, A. Ingemarsson, and J. Mahalabanis, Phys. Rev. C **46**, 1974 (1992).

[19] F. Carstoiu and R. J. Lombard, Phys. Rev. C **48**, 830 (1993).

[20] G. Bertsch, H. Esbensen, and A. Sustich, Phys. Rev. C **42**, 758 (1990).

[21] J. P. Jeukenne, A. Lejeune, and C. Mahaux, Phys. Rev. C **16**, 80 (1977).

[22] F. Carstoiu and M. Lassaut, Nucl. Phys. **A597**, 269 (1996).

[23] R. Anne *et al.*, Nucl. Phys. **A575**, 125 (1994).

[24] M. Lassaut and R. J. Lombard, in *Proceedings of the VIth International Conference on Nuclei Far from Stability and IXth International Conference on Atomic Masses and Fundamental Constants*, Bernkastel-Kues, 1992, edited by R. Neugart and A. Wöhr, IOP Conf. Proc. No. **132** (Institute of Physics and Physical Society, London, 1993).

[25] W. A. Friedman, Phys. Rev. C **27**, 569 (1983).

[26] J. Hüfner and M. C. Nemes, Phys. Rev. C **23**, 2538 (1981).

[27] M. S. Hussein and K. W. McVoy, Nucl. Phys. **A445**, 124 (1985).

[28] B. A. Brown, A. Csótó, and R. Sherr, Nucl. Phys. **A597**, 66 (1996).

[29] F. C. Barker, Nucl. Phys. **A588**, 693 (1995).

[30] C. W. Johnson, E. Kolbe, S. E. Koonin, and K. Langanke, Astrophys. J. **392**, 320 (1992).